UNIVERSITY OF CALIFORNIA
SANTA CRUZ

BICYCLE WHEEL SYSTEM IDENTIFICATION AND OPTIMAL TRUING

A thesis submitted in partial satisfaction of the
requirements for the degree of

MASTER OF SCIENCE

in

COMPUTER ENGINEERING

by

Aaron M. Hunter

June 2021

The Thesis of Aaron M. Hunter
is approved:

Professor Gabriel Elkaim, Chair

Professor Dejan Milutinovic

Professor Michael Wehner

Quentin Willians
Acting Vice Provost and Dean of Graduate Studies

Table of Contents

List of Figures

List of Tables

Abstract

Bicycle Wheel System Identification and Optimal Truing

by

Aaron M. Hunter

The spoked bicycle wheel is one of the most ubiquitous tensioned structures in the world and its assembly and tensioning is largely automated. Nevertheless, the algorithms employed in the tensioning process are heuristics that essentially mimic a skilled human worker. While these heuristic can yield very well-tensioned wheels, they are not efficient and occasionally do not converge, requiring manual intervention.

This work describes an *in-situ* empirical modeling technique of a conventional bicycle wheel employed to determine the optimal tension adjustments necessary to align the wheel in lateral and radial directions while targeting a desired uniform spoke tension. The technique allows the mean tension of the spokes to be adjusted independently from variations around the mean. Additionally, a control algorithm is developed that uses lateral feedback and predicted intermediate wheel states to bring the wheel into alignment to the desired tension in a single iteration of adjustments of the tension of the spokes. First the method is simulated on randomly tensioned wheels. Then the algorithm is demonstrated experimentally on an actual bicycle wheel.

To my wife,

Natasha Perry,

who set aside her dislike of clutter in order for me to complete this work.

Acknowledgments

I want to thank Stuart Davis for the initial inspiration of this work and Dr. Matt Ford for his enthusiastic support during its development.

Chapter 1

Introduction

1.1 Introduction

This work documents a method for determining the optimal tension of the spokes of a bicycle wheel to meet its desired specification and a method for adjusting the spoke tension to achieve that specification. Specifically, we model the effect of a unit change in spoke tension on the measured parameters of the bicycle wheel, namely rim displacement and tension of all the other spokes. and provide for an optimal tensioning method for all wheels of the same type. Although we performed all the experiments by hand, this work is intended for integration into an automated wheel manufacturing apparatus equipped with the appropriate sensors.

1.2 Motivation

Motivation for this work came from conversations with manufacturing personnel at a Santa Cruz, California bicycle manufacturer. They contacted the Autonomous Systems Lab

because they wanted to improve the performance of their automated, state of the art, wheel tensioning machines and to minimize the occurrence of manual interventions necessary when the machines failed to achieve the desired specifications. We also corresponded with the manufacturer of the machines and observed the machines in operation. These interactions revealed that the algorithm used to tension the wheels is an iterative method based on a geometric heuristic–much like that of a human operator–and that this heuristic is not guaranteed to converge to an optimum solution. Both the non-optimality and the cost of manual intervention increase the cost of producing a wheel. The goal of this study is to provide a deterministic, optimal method to true a bicycle wheel that improves upon the performance of the iterative method and eliminate the need for manual intervention.

1.3 Related Work

The spoked bicycle wheel is one of the most ubiquitous tensioned structures in the world. While much has been written about modeling the structure itself ([13], [3], [11], [7], [14], [6]) very little has been published regarding the assembly and tensioning (known as 'truing') of the wheel. Brandt [2] offers one of the first finite element models of the wheel and provides a heuristic to true the wheel that first minimizes lateral errors, then radial errors, then increases the tension of all the spokes and iterates the process up to a maximum mean spoke tension. Papadaplous [12] received a patent for an algorithm to determine the optimal spoke tension adjustments using a linear least squares approach, however doesn't provide a method for implementing the solution nor does it allow for targeting an arbitrary mean tension. That

is, he provides a truing solution only at the current mean spoke tension. Finally, Jambor [9] offers a method to determine the spoke tensions necessary to true a wheel using a finite element model, but this approach requires full knowledge of the wheel component properties and also doesn't implement a method for truing the wheel.

1.4 Contributions

This thesis contributes to the state of the art in the following areas. We provide a method of system identification of the spoke tension on the measurable properties of a wheel. We develop a linear model that predicts the state of the wheel given a set of spoke tension adjustments using the identified system. We develop a method for determining the optimal set of adjustments needed to meet any achievable specification (including changing the mean tension) of the wheel. Finally, we demonstrate an algorithm that applies those adjustments while minimizing the errors that occur during the tensioning process. Along the way we also develop a method to digitize analog gauge measurements using computer vision techniques and demonstrate measurement precision that exceeds the nominal resolution of the instrument. Much of this work appears in [8]).

1.5 Thesis Organization

This thesis is developed in four parts. After this introductory chapter we delve into details of the work itself.

In Chapter 2, we introduce the wheel structure, define the wheel state and identify

the forces that affect the wheel state. Then we introduce the measurement apparatus and the experimental wheel. We then define a model of the wheel as a matrix that transforms the wheel from its current state to a new state based on a vector of spoke tension changes. We conclude with the formulation of the problem as a weighted, multi-objective, least-squares estimation of the optimal spoke tension vector.

In Chapter 3, we present the simulated and experimental validation of the methods. The first experiment is a simulation of effect of different models. The second is an experimental validation of the model using the simulation results. The third and fourth experiments demonstrate the optimal tensioning of a randomly de-tensioned wheel.

In Chapter 4 we present our conclusions and discuss future areas for development.

Chapter 2

Method

2.1 Background

The bicycle wheel structure consists of a rim, spokes, spoke nipples, and a hub. Fig. 2.1 shows a side view of the wheel and Fig. 2.2 shows the rim cross section. The hub anchors each spoke which in turn tensions the rim via a threaded nipple seated in the rim. The rim is tensioned to its desired value by tightening or loosening the nipples. A wheel has n spokes located at equal increments around the rim defined by their location $\theta_i,\ i \in [1,2,\ldots,n]$,

$$\theta_i = \theta_0 + (i-1)\frac{n}{2\pi} \tag{2.1}$$

and θ_0 represents the location of the valve stem as a fixed reference point.

The spokes are offset from the plane containing the rim by the spoke angles α_{nd} and α_d. The angle partitions the spoke tension into two components, a radial component and a lateral one as also seen in Fig. 2.2. Radial tension provides the wheel its ability to carry a load by putting the rim under compression. As long as the spokes remain under tension the wheel

will support a load. The lateral component of the spoke tension provides a means to adjust the lateral displacement of the rim in the plane of the wheel that result from natural variations in the mechanical properties and geometry of all the components. The optimal tension of the wheel is a balance between the two, that is, high enough radial tension to support the anticipated load, but below the lateral value that exceeds the rim stiffness, which induces rim buckling [5]. Note that there are two other degrees of freedom for rim displacements: tangential, that is along the rim circumference and torsion around the rim shear center. The former merely results in a rotation of the rim around the axle and is therefore not of interest here.The latter is a concern for wheels containing spokes that are significantly offset from the rim center and therefore generate a twisting moment. In this work we assume that any torsion effect is minimized when the lateral and radial variations are minimized. In practice, this effect is primarily reduced through appropriate rim design.

Spoking patterns vary from radial to nearly tangential relative to the hub and determined by angle β. Tangential spoke patterns allow for torque transmission from the hub to the rim due to the drive train or disc brakes. With the exception of some lightweight front wheels on bicycles with rim brakes, all wheels are built with some degree of tangential spoking. We define a location along the rim by its angle θ as defined earlier for the spokes.

Truing is the process of adjusting the spoke tension to minimize the lateral and radial variations of the rim while maintaining uniform spoke tensions. The ideal wheel is perfectly round and has the rim lie in a flat plane perpendicular to the ground, so truing is done to minimize the variations away from the ideal wheel. As can be seen in Fig. 2.2, increasing the tension of a spoke generates a lateral force, which pulls the rim towards the spoke, and a radial force,

pulling the rim towards the center of the wheel. The typical procedure for wheel truing by hand is a heuristic where first all the spoke nipples are tightened to tension the wheel, then the lateral variations are iteratively reduced, followed by the radial variations. The wheel tension is then increased incrementally and the procedure is repeated until the wheel parameter specifications are met [2].

Provided the materials of the wheel are maintained in their respective linear elastic regions, the wheel is a linear structure. Therefore, wheel parameter variations (in other words, the lateral and radial displacements and the tension values) induced by changes in the spoke tensions can be decomposed into the changes induced by each spoke and superposed, lending itself to influence matrix approach developed in this work.

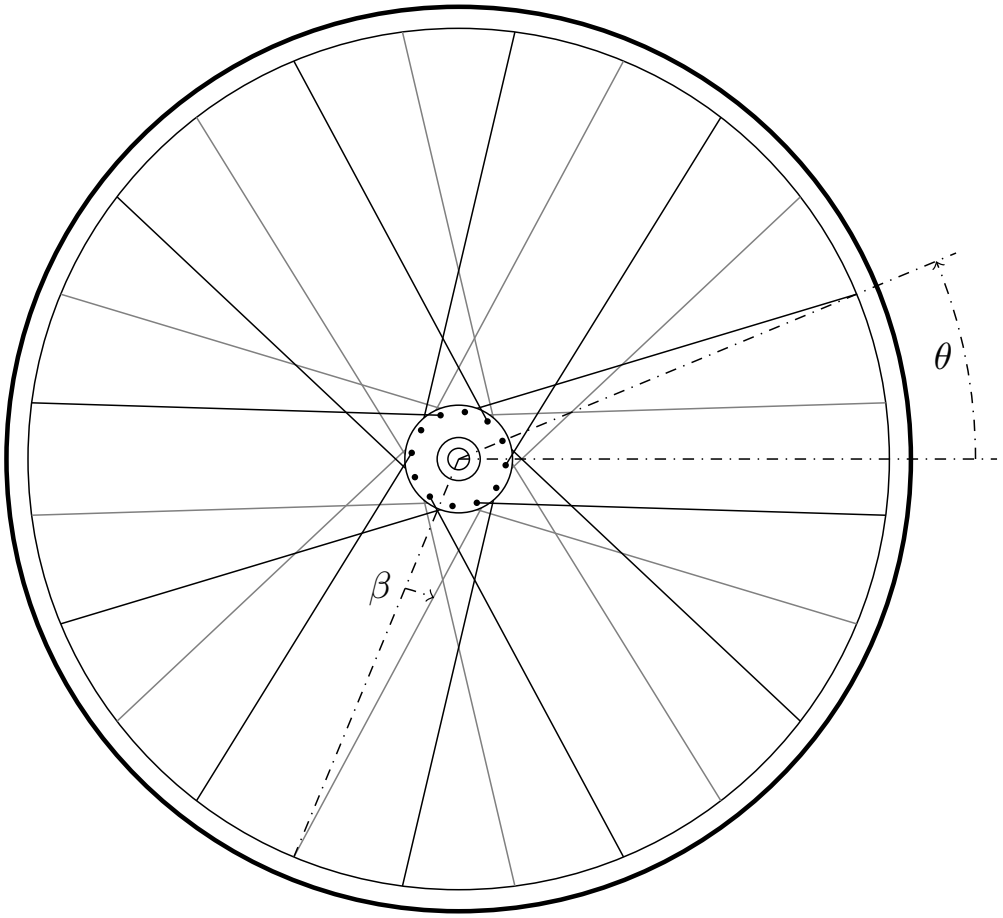

Figure 2.1: Wheel geometry. Side view of a wheel. We define the rim angle, θ, to define a location on the rim. The angle, β, results from the wheel spoke pattern. Torque transmission from the hub to the rim (from either the drive train or disc brakes) requires $\beta \neq 0$. A purely radially spoked wheel ($\beta = 0$) is found only on front wheels with rim brakes .

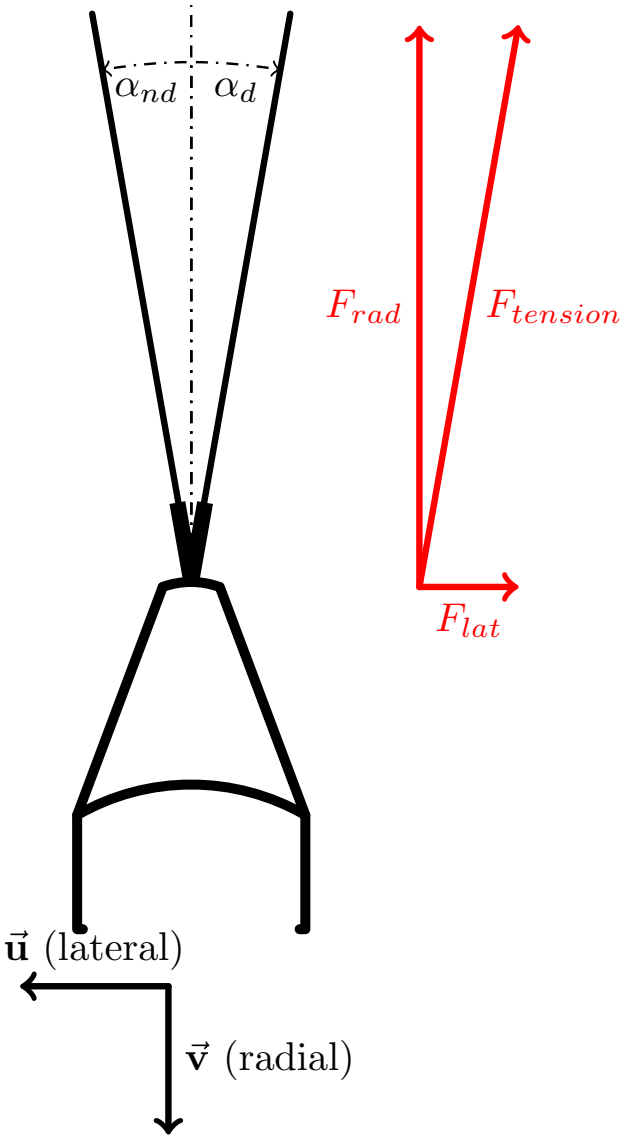

Figure 2.2: Wheel geometry. Rim cross section. The lateral direction (denoted by $\tilde{\mathbf{u}}$) is defined to point toward the non-drive side of the wheel. The radial direction ($\tilde{\mathbf{v}}$) points outwards from the hub. The spoke angles α_d and α_{nd} (where the subscript denotes drive or non-drive side spokes) provide for lateral truing of the wheel and can be different from each other depending on the wheel type. Increasing the tension of a spoke on the drive side results in radial force inward and a lateral force towards the spoke. *Truing* is the process of adjusting the tension so that the wheel is round and the rim is straight, that is, it lies in a flat plane.

2.2 Apparatus

A Centrimaster truing stand was used for all the truing operations and rim displacement measurements. It has a bearing surface contacting the rim sidewall that is connected to an analog depth gauge to measure radial displacements. It has a similar depth gauge contacting the rim edge to measure radial displacements. Both gauges have scale resolution of 0.1mm, although interpolation between the markings allows for better precision. A Canon EOS-M camera with a 22mm macro lens was used to capture the images used to digitize the analog gauge measurements and interpolate between scale markings. We performed all the experiments on a hand-built road bicycle wheel consisting of a Stans ZTR Alpha rim, DT Swiss butted stainless steel spokes and a Wheelsmith hub. The measurement setup is shown in Fig. 2.3. A WheelFanatyk digital tensiometer (not shown) provided all spoke tension measurements.

Figure 2.3: Measurement setup of the Centrimaster truing stand, digitization camera and tripod. The test wheel used for all the experiments is mounted in the truing stand. Not shown is the WheelFanatyk tensiometer used to measure spoke tension.

2.3 Problem Formulation

A wheel with n spokes has tension adjustments represented by an $n \times 1$ vector $\mathbf{d}$. We would like to find the least-squares estimation of the spoke adjustment vector, $\hat{\mathbf{d}}$, that most closely solves following relation,

$$\mathbf{Y} = \Phi\hat{\mathbf{d}} + \mathbf{e} \tag{2.2}$$

Where $\mathbf{Y}$ is a $3n \times 1$ vector defined as the measured wheel state (which we'll elaborate on in the next section), Φ is a $3n \times n$ matrix representing a discrete model of the system, and $\mathbf{e}$ is a $3n \times 1$ vector of random measurement error. We find the optimal estimate of $\hat{\mathbf{d}}$, in the least-squares sense, by constructing a cost function J which is the sum of the squares of the measured wheel state minus the prediction:

$$J = (\mathbf{Y} - \Phi\hat{\mathbf{d}})^T(\mathbf{Y} - \Phi\hat{\mathbf{d}}) \tag{2.3}$$

We minimize J by taking the partial derivative of J with respect to $\hat{\mathbf{d}}$ setting it to zero and solving for $\hat{\mathbf{d}}$,

$$\frac{\partial J}{\partial \hat{\mathbf{d}}} = 0 \tag{2.4}$$

$$\frac{\partial}{\partial \hat{\mathbf{d}}}\left(\mathbf{Y}^T\mathbf{Y} - 2\mathbf{Y}^T\Phi\hat{\mathbf{d}} + \hat{\mathbf{d}}^T\Phi^T\Phi\hat{\mathbf{d}}\right) = 0 \tag{2.5}$$

$$-2\Phi^T\mathbf{Y} + 2\Phi^T\Phi\hat{\mathbf{d}} = 0 \tag{2.6}$$

$$\Phi^T\mathbf{Y} = \Phi^T\Phi\hat{\mathbf{d}} \tag{2.7}$$

$$\implies \hat{\mathbf{d}} = (\Phi^T\Phi)^{-1}\Phi^T\mathbf{Y} \tag{2.8}$$

$$= \Phi^{\dagger}\mathbf{Y} \tag{2.9}$$

where $\Phi^{\dagger}$ is the pseudo-inverse of Φ. [1]

So far we've assumed that the measurements are all of equal importance with the same units. However, in our case we measure two displacement vectors (the lateral and radial variations) and one tension vector. To account and adjust for their relative importance in the solution we introduce weighting factors, μ_v, and μ_t. These factors account for the different measurement units (and therefore magnitudes) and allow flexibility in weighting the solution towards one specification over the others. There are many methods that accomplish this weighted estimation, however, to keep the form of Eq. 2.9 we define a new measurement vector, $\tilde{\mathbf{Y}}$ and new model, $\tilde{\Phi}$:

$$\tilde{\mathbf{Y}} = \begin{bmatrix} \mathbf{u} \\ \mathbf{v}\sqrt{\mu_v} \\ \mathbf{t}\sqrt{\mu_t} \end{bmatrix} \tilde{\Phi} = \begin{bmatrix} \Phi_u \\ \Phi_v\sqrt{\mu_v} \\ \Phi_t\sqrt{\mu_t} \end{bmatrix} \tag{2.10}$$

Where $\mathbf{u}$, $\mathbf{v}$ and $\mathbf{t}$ are the lateral, radial, and tension measurement vectors respectively, each of length n, and Φ_u, Φ_v and Φ_t are the $n \times n$ matrix sub-models for the lateral, radial, and tension system response. The *weighted* least-squares estimate, $\tilde{\mathbf{d}}$ is then determined from:

$$\tilde{\mathbf{d}} = \tilde{\Phi}^{\dagger}\tilde{\mathbf{Y}} \tag{2.11}$$

2.4 System Identification

Each column of Φ represents the change of the wheel state to the change in tension of a given spoke. What we have not yet discussed is *how* to determine the values of each element

[1] There are many robust mathematical ways to compute the pseudo-inverse of a matrix; the normal equations in Eq. eq:lsq are not normally used beyond the derivation.

of Φ. The approach we develop in the next section treats the system as a black box, that is, we assume that we know nothing about the system except what we can observe and linearity. To determine the system response we make a small change to each input to the system separately and measure the outputs of the system.

The main issue with this approach is that without a specific physical model to fit it is difficult to distinguish the noise from the measurements. To simplify the task somewhat, however, can determine some interesting properties from the geometry of the system. For example, referring to Fig. 2.1, we see that a wheel may have symmetries. We can exploit these by grouping the responses of elements with the same symmetry and fit a single response vector to that group. This fitting can be simple averaging, but a better approach is to observe that each column of Φ can be considered a periodic signal with a period of 2π. Fourier theory states that any periodic signal can be approximated by the Fourier series. The Fourier series takes the form:

$$y(\theta) = a_0 + \sum_{n=1}^{N} a_n \cos(n\theta) + b_n \sin(n\theta) \tag{2.12}$$

where $n\theta$ is the spatial frequency of the mode of oscillation and $y(\theta)$ is the value of the function at angle θ. This is discussed in more detail in the next chapter.

2.5 Wheel Model

Our approach builds upon the methods presented in Papadapolous and alluded to in [1]. It relies on an *in-situ* system identification method to determine the influence of a unit tension adjustment of a spoke on the lateral, radial and tension (that is, the tension of the other

spokes in the wheel) parameters of a specific wheel. This is referred to as the *influence function* of a given spoke and forms one column vector of Φ defined in the previous section. The superposition of the individual influence functions of the all spokes form the complete model of Φ for how the vector, **d**,of tension adjustments changes the entire state of the wheel. Φ is referred to as the *influence matrix*. A given wheel that is out of alignment and non-uniformly tensioned is modeled as a linear combination of spoke tension adjustments relative to a perfectly trued wheel at the same average tension using a weighted least squares estimation. Where this algorithm improves upon previous approaches is to provide tension targeting and a method for feedback control during the tensioning process to minimize cumulative adjustment errors.

To develop the model of the wheel we first determine experimentally the effect of a unit tension change of a spoke on the lateral and radial rim displacements as a function of rim angle of a wheel and the tension of the other spokes in the wheel. These are the influence functions discussed previously. Once determined, the influence functions are used to model the system behavior given an arbitrary set of spoke tension adjustments using the weighted least squares regression technique outlined in the previous section (this is a common approach to system identification–see for example [10]). For each experiment an initial measurement is taken of the radial and lateral displacements at the spoke angle, θ_i, and the tension of each spoke. The resulting measurements define the initial wheel state. We then loosen one spoke by a fixed rotation to perturb the wheel state and repeat the measurement cycle. The difference between the perturbed state and the initial state is the measured influence function for each wheel parameter of a given spoke (see Fig. 3.2). The influence functions of a given spoke are therefore three vectors of length n. To minimize noise these data are either averaged or fit to

a Fourier series. They are then placed column-wise into three $n \times n$ influence matrices such that each column is the influence function of a given spoke and each row represents a discrete rim angle. In other words, if $u(\theta), v(\theta),$ and $t(\theta)$ are the lateral, radial, and tension influence functions for spoke $i \in [1, 2, \cdots, n]$, then the influence matrices Φ_u, Φ_v and Φ_t for the lateral, radial and tension parameters respectively, at the discrete rim angles $\theta \in [\theta_1, \theta_2, \cdots, \theta_n]$ are given by:

$$\mathbf{u} = \begin{bmatrix} u(\theta_1) \\ u(\theta_2) \\ \vdots \\ u(\theta_n) \end{bmatrix} \mathbf{v} = \begin{bmatrix} v(\theta_1) \\ v(\theta_2) \\ \vdots \\ v(\theta_n) \end{bmatrix} \mathbf{t} = \begin{bmatrix} t(\theta_1) \\ t(\theta_2) \\ \vdots \\ t(\theta_n) \end{bmatrix} \tag{2.13}$$

$$\Phi_u = \begin{bmatrix} \mathbf{u_1} & \mathbf{u_2} & \dots & \mathbf{u_n} \end{bmatrix} \tag{2.14}$$

$$\Phi_v = \begin{bmatrix} \mathbf{v_1} & \mathbf{v_2} & \dots & \mathbf{v_n} \end{bmatrix} \tag{2.15}$$

$$\Phi_t = \begin{bmatrix} \mathbf{t_1} & \mathbf{t_2} & \dots & \mathbf{t_n} \end{bmatrix} \tag{2.16}$$

The influence matrices are the models of the wheel for each parameter. They are combined into the single $3n \times n$ matrix Φ, which is exactly the form we defined in the previous section:

$$\Phi = \begin{bmatrix} \Phi_u \\ \Phi_v \\ \Phi_t \end{bmatrix} \tag{2.17}$$

Now, given a vector spoke tension adjustments, $\mathbf{d}$, and the initial state of the wheel, $\mathbf{Y_0}$, the

predicted final wheel state after applying the adjustments is given by:

$$\hat{\mathbf{Y}} = \mathbf{Y_0} + \Phi\mathbf{d} \tag{2.18}$$

where $\hat{\mathbf{Y}}$ is the predicted state of the wheel after tensioning. This completes the development on the wheel model, Φ.

2.6 Weighted Least Squares Estimation of $\hat{\mathbf{d}}$

To find the optimal vector of spoke tension adjustments, $\hat{\mathbf{d}}$, that transform a perfect wheel into in a measured state, $\mathbf{Y}$, at average tension $\bar{T}$, a weighted least squares approximation is solved using a set of measurements $[\mathbf{u}, \mathbf{v}, \mathbf{T} - \bar{T}]$, and the weights μ_v and μ_t:

$$\tilde{\Phi} = \begin{bmatrix} \Phi_u \\ \Phi_v\sqrt{\mu_v} \\ \Phi_t\sqrt{\mu_t} \end{bmatrix} \quad \tilde{\mathbf{Y}} = \begin{bmatrix} \mathbf{u} - u_0 \\ (\mathbf{v} - v_0)\sqrt{\mu_v} \\ (\mathbf{T} - \bar{T})\sqrt{\mu_t} \end{bmatrix} \tag{2.19}$$

$$\hat{\mathbf{d}} = \tilde{\Phi}^{\dagger}\tilde{\mathbf{Y}} \tag{2.20}$$

Where $\tilde{\Phi}^{\dagger}$ is the pseudo-inverse of $\tilde{\Phi}$ as we defined earlier. Typically u_0 and v_0 are zero reflecting the fact that the gauge has been set to zero at the desired lateral and radial locations during setup.

The weights, μ_v and μ_t, are needed to account for several factors when determining the optimal truing solution. The first and most significant is that tension is measured in Newtons but the spoke displacements are measured in millimeters, so to first order the weighting factors normalize the measurements to a common scale (in this case the lateral measurements).

They also account for the magnitude of the response of each parameter due to a unit tension adjustment. For example, the radial displacement of the rim due to a unit adjustment is much smaller than the lateral displacement, but both parameters typically have the same desired specification (see Fig. 3.2). Similarly, the spoke tension may have a larger relative tolerance and generally is a less precise measurement. Finally, if one type of measurement is inherently noisy or inaccurate its weight is reduced during simulation until the solution is relatively unaffected by the quality of the signal. The weights therefore allow the user the flexibility necessary to meet the specifications of a given wheel. Once $\hat{\mathbf{d}}$ is found the wheel is trued to its optimal state, $\mathbf{Y}_{ls}$ by applying $\mathbf{d}_{adj} = -\hat{\mathbf{d}}$ to the wheel, where the negative sign indicates the direction of the adjustment necessary to "undo" the already imperfectly tensioned wheel.

$$\mathbf{Y}_{ls} = \mathbf{Y}_{\mathbf{0}} + \Phi \mathbf{d}_{adj} \tag{2.21}$$

2.7 Tension Targeting

In theory adjusting a wheel to a desired mean tension is accomplished by setting $\bar{T} = T_d$ in Eq. 2.19, where T_d is the desired tension. As we demonstrate later, however, the tension influence functions are noisy and lack the necessary precision to target tension accurately. Additionally, we are unable to distinguish the small rim diameter compression that occurs with changes of tension from the radial measurements. Therefore we need a better method to simultaneously true and tension a wheel to a tension T_d that is significantly different from $\bar{T}$. For this method we can exploit the wheel symmetry from the following observation. If every spoke of a symmetric ($\alpha_d = \alpha_{nd}$) wheel is tightened by the same amount then the radial and lateral

displacements are unaffected and only the average tension is changed. It is possible therefore to decouple the average tension change from spoke tension non-uniformity.

Formally, what we wish to do is to find the vector, **d**, that minimizes our cost function as before, but with the added constraint that the average radial tension of the wheel is unchanged, that is,

$$\sum_{i=1}^{n/2} d_{nd_i} \cos(\alpha_{nd}) + \sum_{i=1}^{n/2} d_{d_i} \cos(\alpha_d) = 0 \tag{2.22}$$

where we explicitly label the elements of **d** depending on whether they are from the drive-side (d_{d_i}) or non-drive side (d_{nd_i}). For our symmetric wheel this is the same as adding the constraint that the average of the adjustment vector is zero, that is,

$$\bar{d} = \sum_{i=1}^{n} d_i = 0 \tag{2.23}$$

For the general case, however, we solve Eq. 2.22 and compute different values for drive-side and non-drive side contributions to radial tension. What follows is the treatment of the symmetric case as it corresponds to our test wheel and demonstrates the concept adequately. Extending this concept to asymmetric wheels is left as a future development.

The approach is as follows. First calculate $\hat{\mathbf{d}}$ as in Eq. 2.20 and subtract its mean value, $\bar{d}$. This is the spoke adjustment vector which will cause a perfectly true wheel to result in the measured wheel state, without changing $\bar{T}$. As before, **d** is the vector that transforms the wheel to the trued state:

$$\mathbf{d} = -(\hat{\mathbf{d}} - \bar{d}) \tag{2.24}$$

$$\tag{2.25}$$

If the adjustments, **d**, are applied to the spokes, the lateral, radial and tension variations are minimized as before, but the mean tension is unchanged. We determine the necessary constant shift, d_{cm}, to bring the mean tension to T_d by calculating the following:

$$d_{cm} = (T_d - \bar{T})/c \tag{2.26}$$

Where the proportionality constant, c, is the change in the average tension of the wheel when all the spoke nipples are rotated by one revolution. The spoke vector that optimally trues the wheel *and* at the desired tension is:

$$\mathbf{d}_{adj} = \mathbf{d} + d_{cm} \tag{2.27}$$

Finally, to determine c, we measure the change in average tension of a wheel where we add a constant adjustment d_{cm} to *all* the spokes in the wheel. In this work we measure the average tension for various values of d and calculate the least squares fit of the $\bar{T}$ to d_{cm} following the same approach as developed in Section 2.3.

2.8 Optical Digitization

Although a mechatronic implementation of a wheel tensioning machine would likely use digital gauges, optical digitization of analog gauges is a powerful technique and can result in extremely fine resolution–often more precise than a digital gauge. Therefore, a method for converting the analog dial gauge readings into digital measurements using computer vision merits some discussion. Prior to taking measurements two images are collected. The first is a reference image of the gauge with the needles outside the expected data range. The second is

(a) (b) (c) (d)

Figure 2.4: Images used to measure analog dial gauges with computer vision. (a) Reference image with the needles away from the normal range of the gauge. (b) Measurement image (in this case at the zero position). (c) Result of the subtraction of the measurement image from the reference image. (d) After masking (concentric rings) and thresholding operations. The angle of the needles in the masked area is measured relative to the gauge center and the converted to a displacement measurement.

of the gauge with the needles set to zero. With these two images any subsequent image of a measurement is processed in the following manner. The measurement image is subtracted from the reference image after appropriate smoothing (to minimize noise). The images are taken under the same lighting conditions, therefore what remains after subtraction is a ghost image of the needles themselves. A binary threshold is applied to the subtracted image and masked to show the tips the needles. Finally, the centroid of the needle tips are determined and the angle from the gauge center to the tip is calculated and compared to the zero measurement image. The angle is then converted into displacement using the gauge resolution. This process is demonstrated in Fig. 2.4.

2.9 Wheel Truing Algorithm

Having determined the optimal spoke adjustments, $\mathbf{d}_{adj}$, the remaining task is to apply them to the wheel. Although this sounds deceptively simple, there are some difficulties doing this accurately. The main one is a problem of spoke twist. Spokes are not torsionally stiff and will twist significantly during nipple rotation. Thus it is difficult to determine precisely how far the spoke nipple has been adjusted based entirely on the rotation angle of the spoke nipple. Actuator accuracy or precision may also be inadequate, leading to the accumulation of errors over multiple spoke adjustments. This is particularly true at higher spoke tensions where the friction of the nipple-spoke interface can cause discrete jumps in nipple rotation because of the higher adjustment torque required to overcome the friction. Finally, even if the nipple has been adjusted properly but the spoke is twisted, over time it can untwist resulting in a gradual loosening of the spoke and causing the wheel to go out of true.

Although the use of high precision servos and clamping the spoke during adjustment can improve the wheel truing process, we developed a method that minimizes these sources of variability using lateral measurement feedback during the adjustment. The essential idea of the method is that we predict the wheel state after each individual spoke adjustment using the influence matrices and the spoke adjustment value. Rather than adjust the spoke nipple a fixed rotation, instead it is adjusted until the lateral measurement at the rim location of that spoke agrees with the prediction. In other words, the spoke tension is adjusted until the *predicted* state is measured. Note that this predicted intermediate state is *not* the final state of the wheel at this location. The subsequent adjustment of the remaining spokes also affect the displacement

of the rim at this location. The power of the method is the ability to predict the intermediate states during the truing process that ultimately results in a true wheel. The lateral feedback is used because it is the parameter with the highest sensitivity to spoke tension. Spoke twist is minimized simultaneously using the lateral feedback to estimate the hysteresis in the adjustment and adjusting the spoke to the midpoint of the hysteresis band.

The following sequence of operations describes the complete truing method. First measure the initial state of the wheel. Then compute the spoke adjustment vector, **d**, using the weighted least squares algorithm. Next, using Eq. 2.18, predict the lateral wheel state after each adjustment following a pre-defined sequence, spoke $i = 1, 2, \ldots n$. The lateral displacement target for spoke i is the predicted state after the i^{th} adjustment. Starting with first spoke, adjust the nipple until the gauge measurement agrees with the lateral target. Finally, eliminate spoke twist by measuring the spoke rotation hysteresis during adjustment (also using the lateral gauge feedback) and set the spoke nipple angle midway in the hysteresis regime. Repeat this sequence of steps for the remaining spokes until all the spokes have been adjusted. This is demonstrated in the flowchart in Fig. 2.5. Fig. 2.6 shows the predicted lateral states of a wheel after each spoke adjustment along with the lateral targets (diamond symbols). These targets were used to true the wheel for the experiment shown in Fig. 3.11 in the next section. The dashed line represents the lateral state of the wheel prior to tuning, the thin lines show each intermediate state prediction, and the thick line is the prediction of the final state. In practice some adjustments are too small to perform and can be safely ignored if the wheel state at that spoke is already near the target value within an acceptable tolerance.

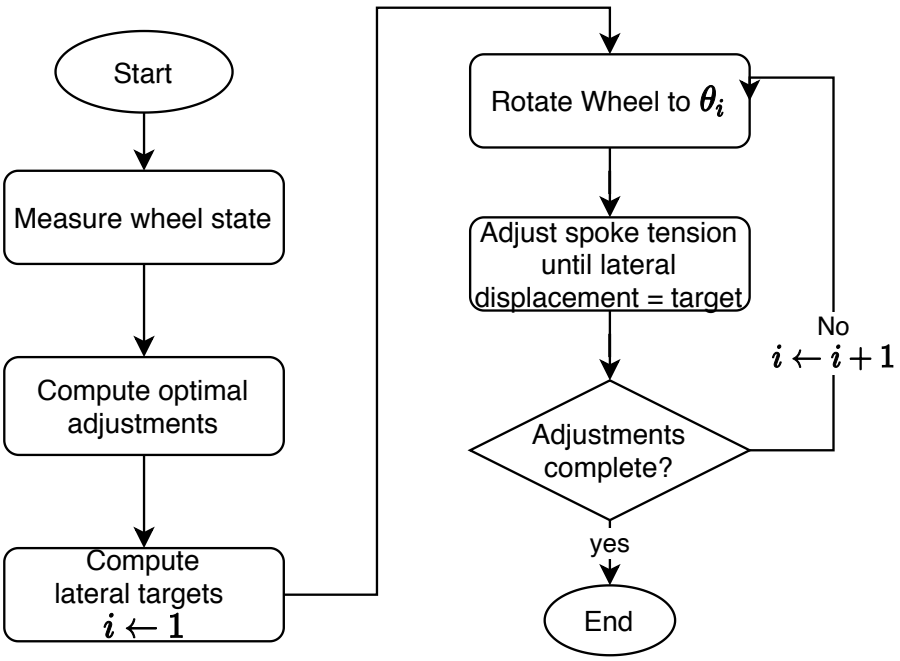

Figure 2.5: Truing algorithm flowchart.

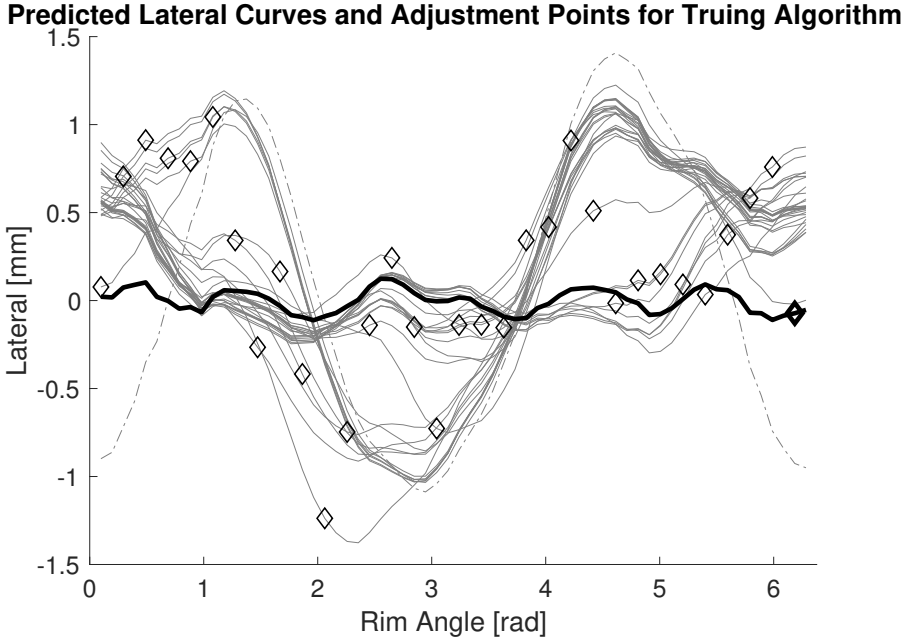

Figure 2.6: Example of the truing algorithm. The dashed line is the initial lateral state. The thin lines are the predicted states after each spoke adjustment. The diamonds are the lateral target values.The spoke tension is adjusted until the lateral measurement agrees with the target and proceeds from the first spoke (leftmost) to the last. Note that the diamond targets do not represent the final wheel state, but the intermediate state after each tension adjustment at that position. The thick line is the predicted final state with its truing target.

Chapter 3

Results

3.1 Optical Digitization of Lateral and Radial Measurements

To validate the computer vision algorithm described in the previous section, we evaluated the measurement reliability using a series of four images. We first analyzed their readings manually (through pixel level measurement of the angle of the needles) and then compared against the results returned by the algorithm. We set both dial gauges to approximately the following settings: 1.0 mm, 0.5 mm, 0.25 mm, and 0.0 mm. Fig. 3.1 shows the comparison between the two methods. The estimated effective displacement resolution of the manual measurement method is approximately 0.014 mm. The computer vision algorithm returned values within $\pm$0.007 mm of the manual measurements.

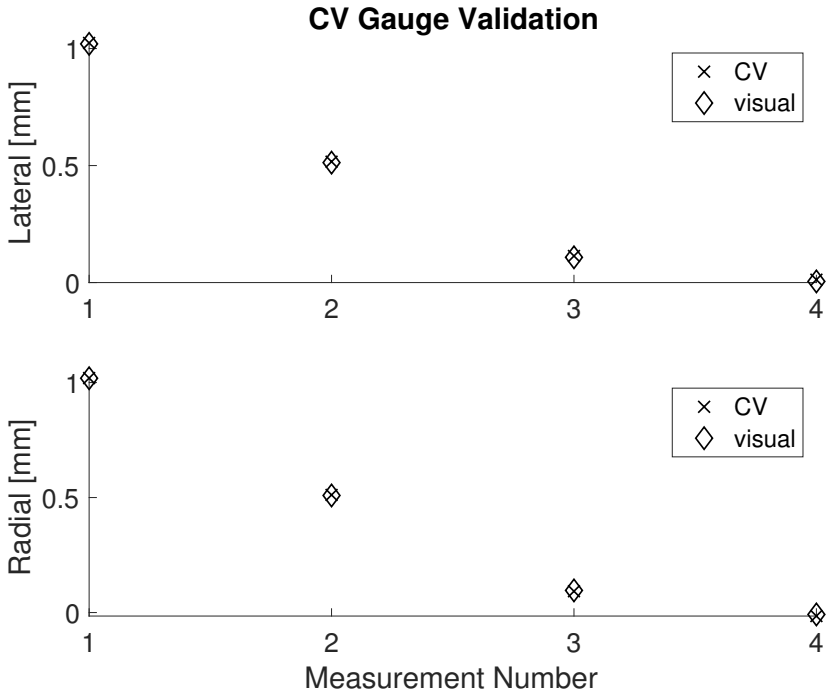

Figure 3.1: Validation of the computer vision algorithm developed to interpret analog dial gauge measurements. The results of the two approaches are within the estimate of the resolution of the manual technique.

3.2 Influence Functions

We measured influence functions for every spoke, 32 in total. For each influence function we measured the lateral and radial displacements at 64 equally spaced locations on the rim starting at the first spoke. To minimize spoke twist in the estimation of the rotation, we marked the spokes and nipples prior to the rotation. We averaged the curves (after rotating them to the same rim angle) and in the case of the radial displacement, subtracted the mean value. The subsequent influence functions are shown in Fig. 3.2. For each tension influence function we measured the tension of every spoke, thus each tension influence function has 32 measurements. This particular spoking geometry results in four distinct tension patterns,

depending on whether the spoke is on the drive side of the wheel, or the non-drive side, and whether it is a 'leading' spoke or a 'trailing' spoke, that is, whether its spoke angle, β, is positive or negative (see Fig. 2.1). Because this is a symmetric wheel, however, the non-drive side leading spoke influence function is a mirror image of the drive side trailing one. Similarly, the non-drive side trailing spoke influence function is a mirror image of the drive side leading one. We exploited this symmetry to generate the four tension influence functions in Fig. 3.4, such that each function represents the average of 16 measured curves and is mirrored when necessary.

We fit the lateral and radial influence functions to the Fourier series Eq. 2.12 as discussed earlier and shown again for convenience.

$$y(\theta) = a_0 + \sum_{n=1}^{N} a_n \cos(n\theta) + b_n \sin(n\theta)$$

To identify the correct order of the model, that is the highest spatial frequency of these functions we randomly divided the set of measured influence functions into two sets, a modeling set and a testing set. We fit the modeling set to the Fourier series to find the coefficients a_n, b_n using least squares. We determined the highest significant spatial frequency by plotting the sum squared residual error between the modeling and testing sets against the number of fitting coefficients, and therefore spatial frequency. This is plotted in Fig. 3.3. It is evident from this plot that the residual error for the lateral influence function is reduced in the testing data set up to a spatial frequency, $N_{lat} = 6$ (i.e., 13 fitting coefficients) and up to $N_{rad} = 13$ (27 fitting coefficients) for the radial influence function. Because the mean influence functions of Fig. 3.2 exhibit little noise, we used them for the model in this work. To make this method practical, however, fewer

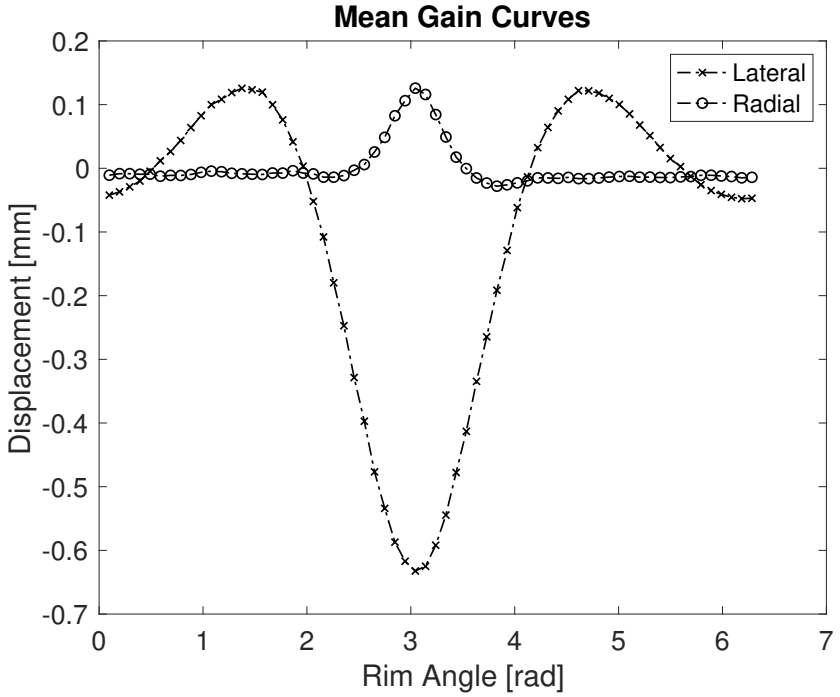

Figure 3.2: The mean influence functions for the lateral and radial parameters. These functions are the average of 32 measured curves after rotating them to the angle of the 16th spoke.

sets of data would be taken and the influence functions would be developed using the Fourier fitting technique.

The tension measurements were noisy and imprecise so they were difficult to fit to a Fourier series with any confidence, therefore, we simply used the averaged data for the tension influence matrix.

Regardless of whether the model or the data are used in the influence functions, however, the influence matrices composed of those functions will be less than full rank. This is because the highest order spatial frequency that appears in the model is 13, corresponding to 27 basis vectors associated with the Fourier coefficients. The wheel, though has 32 independent inputs, that is, spokes. This satisfies an intuitive understanding of the wheel structure, namely

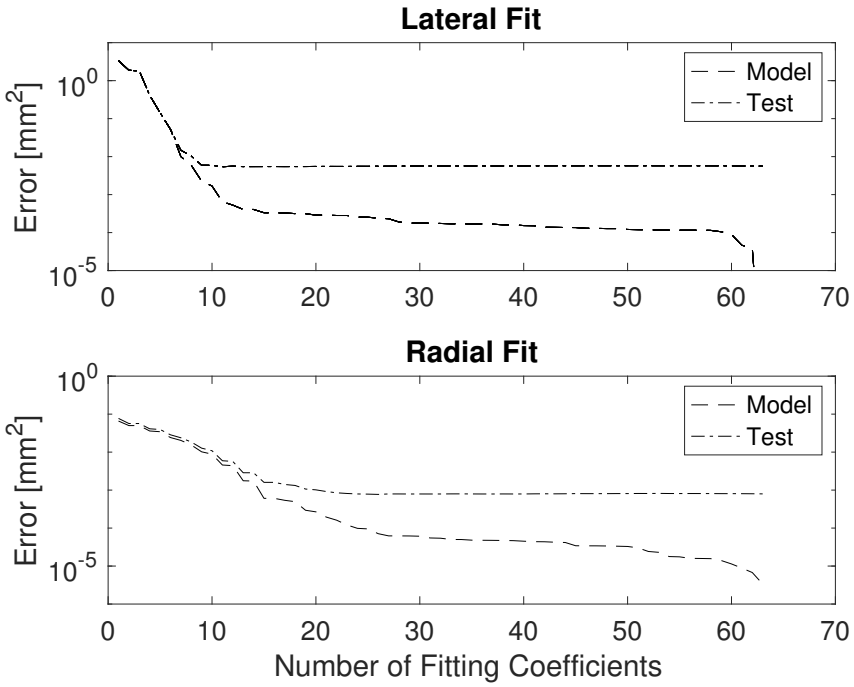

Figure 3.3: Residual error vs fitting coefficient number for the lateral and radial influence functions when fit to a Fourier series. We used the residual of the testing set to determine the highest spatial frequency to be used for the model. Although difficult to discern due to the log scale, the residual error increases in the lateral testing set for fitting coefficients beyond 13, corresponding to $N_{lat} = 6$. Similarly we determined the highest mode of oscillation for the radial influence function to be $N_{rad} = 13$.

that the mean tension of the wheel can be changed without affecting any of the displacement parameters and thus has an infinite number of solutions. This is due to the fact that there are two degrees of freedom that are not taken into account in the wheel model, namely the tangential and torsional modes of the rim.

We verified this independently with a singular value decomposition of the influence matrices composed of solely averaged data for the influence functions, shown in Fig. 3.5. It is evident that without the inclusion of the tension influence matrix the model of the wheel is under-determined.

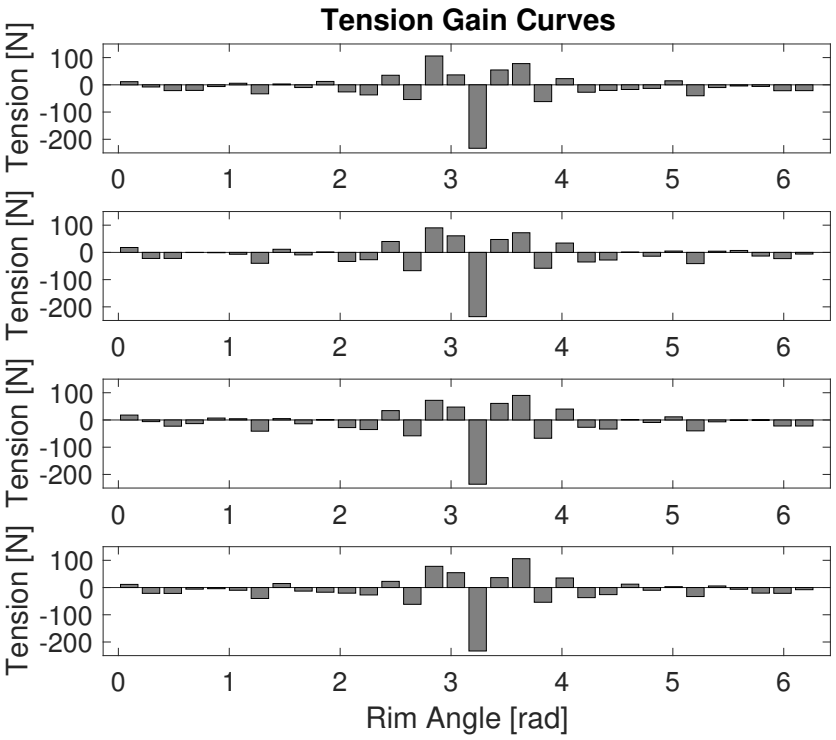

Figure 3.4: The mean influence functions for spoke tension. From top to bottom: (a) Non-drive side leading. (b) Drive-side leading. (c) Non-drive side trailing. (d) Drive side trailing. Note that (a) and (d) are mirror images, as are (b) and (c).

3.3 Simulation

With the influence matrices developed as in Eq. 2.17 we can predict the state of the wheel for a given spoke tensioning vector. To predict d_{ls} however, the weighting parameters μ_v and μ_t need to be determined through simulation. Additionally, given the relatively noisy and coarsely discretized influence functions discuss in the previous section, we simulated an alternative approach for finding d_{ls} using a regularization technique.

Regularization is the process of concatenating the identity matrix in place of the ten-

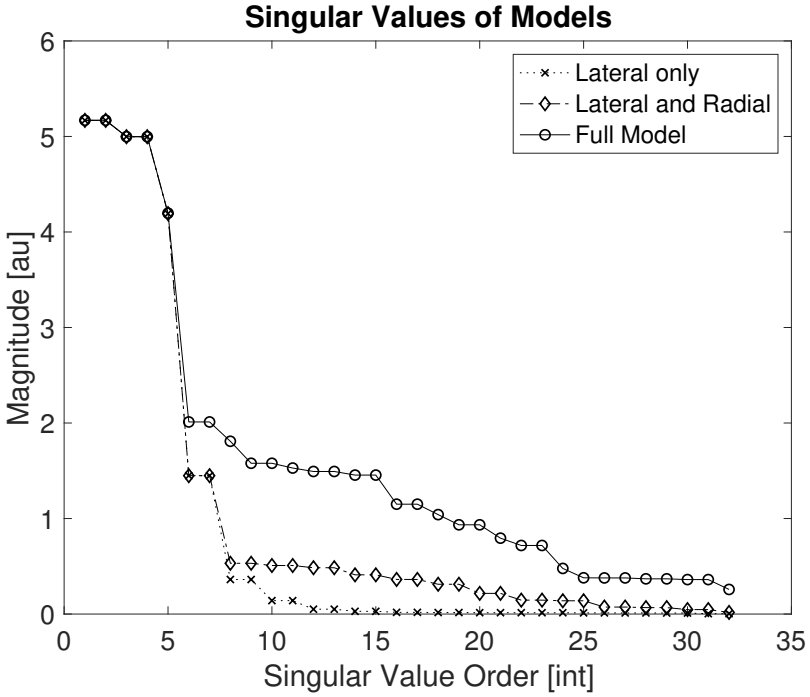

Figure 3.5: The singular values associated with the singular value decomposition of the following influence matrices: lateral, the concatenation of the lateral and the radial, and the full model.

sion influence matrix in $\tilde{\Phi}$ and the zero vector in $\tilde{\mathbf{Y}}$ in place of the tension measurements:

$$\tilde{\Phi} = \begin{bmatrix} \Phi_u \\ \Phi_v \sqrt{\mu_v} \\ I\mu_I \end{bmatrix} \quad \tilde{\mathbf{Y}} = \begin{bmatrix} \mathbf{u} - u_0 \\ (\mathbf{v} - v_0)\sqrt{\mu_v} \\ \mathbf{0} \end{bmatrix} \tag{3.1}$$

where μ_I is a weighting factor for the identity matrix. Regularization has the effect of minimizing $||\mathbf{d_{ls}}||$ when solved for as in Eq. 2.20. The hypothesis for this technique is that the value of $||\mathbf{d_{ls}}||$ that is the smallest is the one that also will minimize tension variations in the solution.

We performed simulations for both the regularized influence matrices, as well as the full model in order to determine the weighting factors. For each simulation a random vector of spoke adjustments was generated and wheel state prediction was calculated using Eq. 2.18.

White noise was added to simulate the uncertainty of the measurement of the wheel state and the noise distributions were determined from the measured profiles generated during the influence function development. The initial weighting factors were developed by normalizing the magnitude of the disturbance of each parameter relative to desired specification, chosen here to be ± 0.1mm lateral, ± 0.05mm, radial, and 1000 ± 100N, tension. The weighted least squares estimation of the random spoke vector $\mathbf{d_{ls}}$ was computed using these weighting factors and the final state of the wheel using Eq. 2.21 was predicted. The weighting factors were modified until the predicted performance error of each algorithm was minimized relative to actual spoke adjustment vector. Fig. 3.6 shows the result of one such simulation. In general the full model outperformed the regularized model by at least a factor of two. The predicted spoke vector for the full model generally agrees to an rms of ≤ 0.1 revolutions. Under iterative simulation we found acceptable weighting factors of: $\mu_v = 0.5$, $\mu_t = 10^{-5}$(mm/N). The small value for μ_t reflects the initial scaling of the unit disturbance between the lateral and tension parameter (0.6mm to 250 N) as well as de-weighting the tension influence matrix due to its noise and imprecision.

3.4 Model Validation

The model is separated into two parts, spoke adjustments which true the wheel but leave the mean tension unchanged, and adjustments which affect the mean tension of the wheel but do not affect the rim displacement parameters. We found the latter part of the model by determining the coefficient, c, between the average of the spoke adjustment vector and the

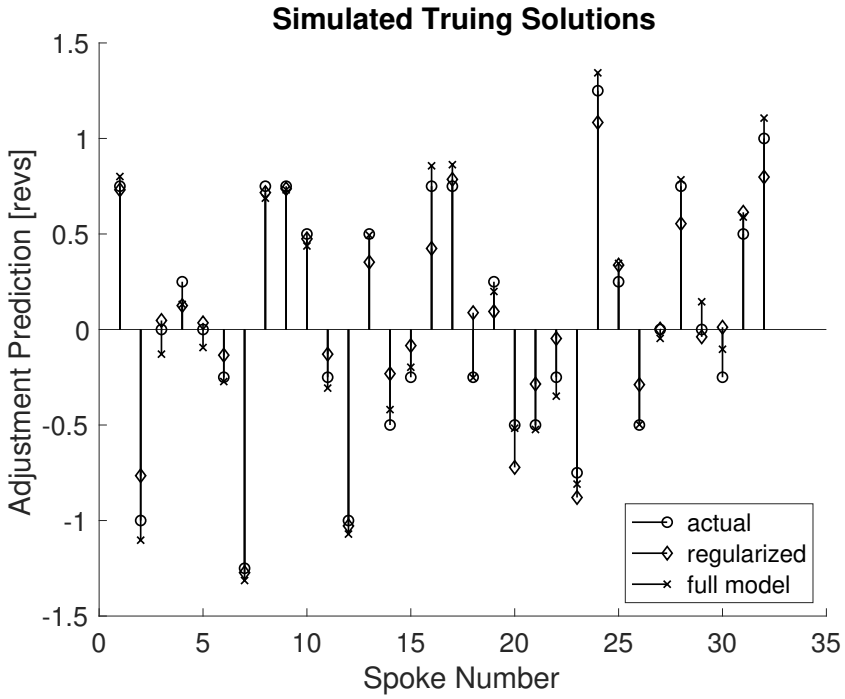

Figure 3.6: Example of the simulation process used to determine the weighting factors for the multi-objective least squares approximation. The circles represent the actual spoke adjustments for a given simulation and the other symbols represent the approximations from two different approaches: a regularized model and the full model. On average, regularization resulted in estimation errors $2\times$ worse than when using the full model.

average tension change of the wheel from seven different experiments. Fig. 3.7 demonstrates the results of seven experiments. A linear fit to these data finds $c = 473$ N/rev. In practice, this constant can be derived from a single experiment where every spoke is adjusted by one revolution.

We performed a different experiment to validate the model performance for preserving the mean tension in the solution. In this case we applied a random spoke adjustments vector to the (manually trued) test wheel and compared the resulting measured wheel parameters to the model predictions. Fig. 3.8 shows the result of this experiment. The rms model error of

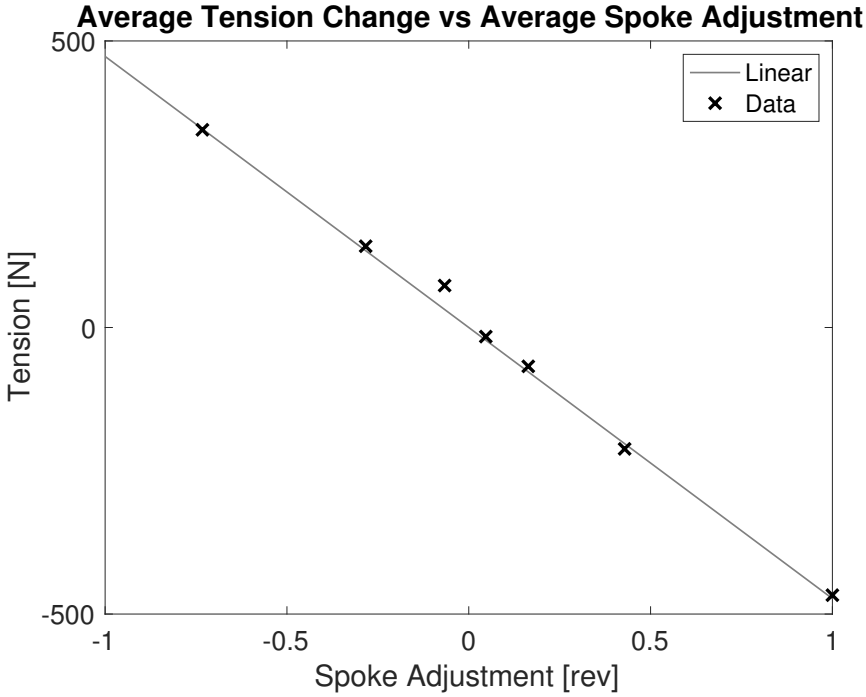

Figure 3.7: The average tension change of a wheel due to the average spoke adjustment. A linear fit to the data finds $c = -473N/rev$.

the lateral, radial and tension parameters are 0.123mm, 0.049mm, and 33N, respectively. The model fits the data well considering the tolerance of the lateral adjustment which is estimated to be 0.1mm.

The need to separate the model into two parts is summarized in Table 3.1 and shown in Fig. 3.10. For this experiment we targeted a well-trued wheel (tensioned to 780N) to a new tension target of 1000N using the original algorithm Eq. 2.19. We applied the resulting spoke adjustment vector to the wheel. Although the wheel is still true the tension exceeds the target by 126N and the tension non-uniformity is 50% worse than the initial state in percentage terms (4.2% vs 6.8%). The reason for the failure of the model in this regime appears to be related to the tension influence functions themselves and is likely due to the relatively large discretization

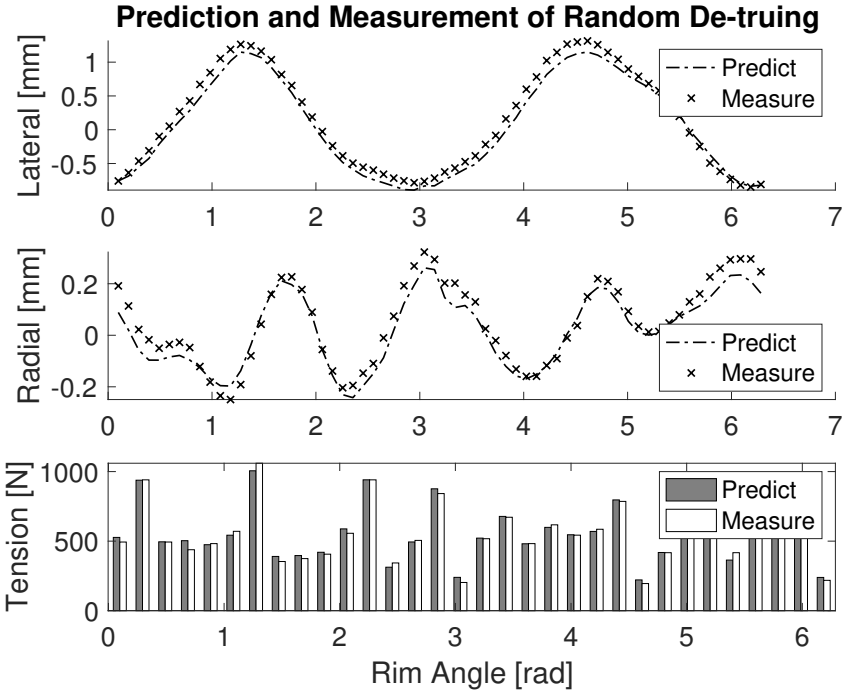

Figure 3.8: The actual and predicted lateral, radial, and tension values for the random de-truing experiment.

errors of the tension measurement (nearly 4% at 1000N). Without finer resolution these discretization errors accumulate when a constant value is added to the spoke adjustment solution. Although better instrumentation and rigorous analysis of the influence functions would likely improve the model, calculating the average tension change separately is a superior solution as the average tension change is easily measured independently.

Table 3.1: Results of Changing Tension

Parameter	Inital ($\mu \pm \sigma$)	Final ($\mu \pm \sigma$)
Lateral [mm]	-0.029 ± 0.083	0.045 ± 0.063
Radial [mm]	-0.052 ± 0.032	-0.056 ± 0.039
Tension [N]	781 ± 33	1126 ± 76

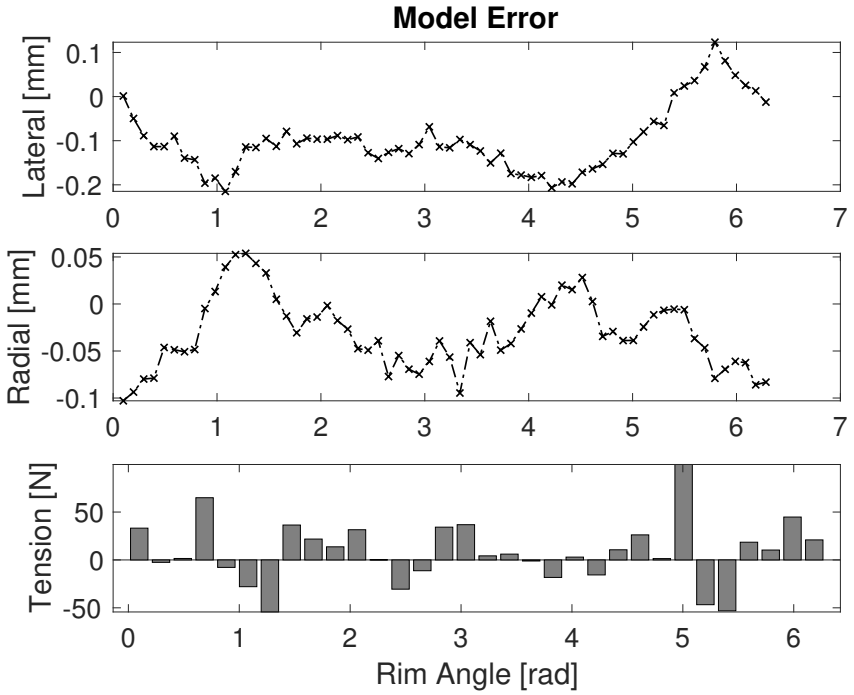

Figure 3.9: The model error relative to the measurements for the random de-truing experiment. The rms errors are found to be 0.123 mm (lateral), 0.049 mm (radial), and 33 N (tension).

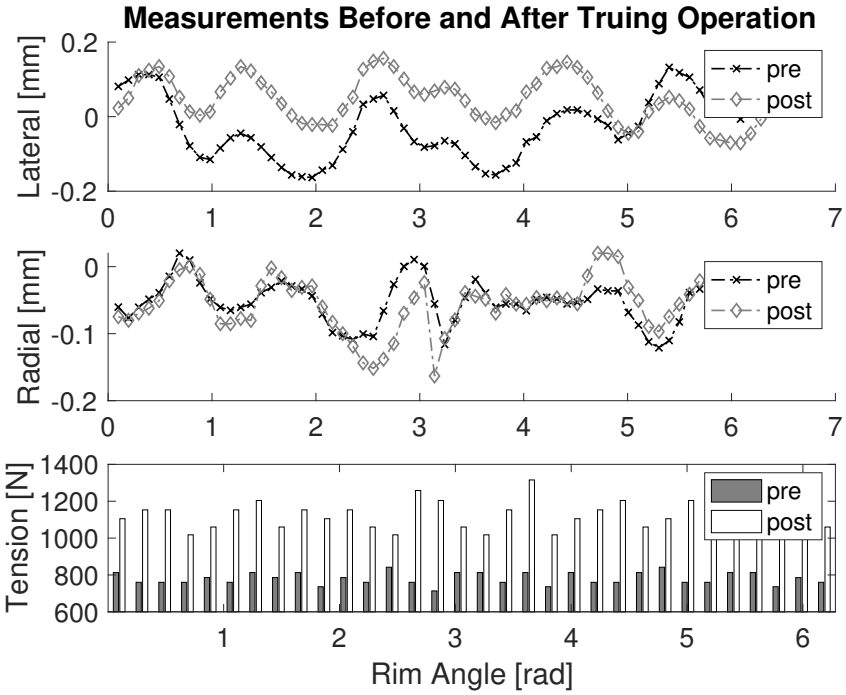

Figure 3.10: Changing the tension of true wheel using the model described by Eq. 2.19. Although the wheel remains true the tension target of 1000N is significantly exceeded and has more variability. This experiment demonstrated the need to target tension independently from tension uniformity and led to the improved algorithm of Eq. 2.27.

3.5 Wheel Truing Validation

To validate the complete model and truing algorithm we applied it to a randomly detrued wheel with a target tension of 1000 N. The initial wheel state was not only substantially out of true, with lateral variations of more than $\pm$1mm, but also at a very low average tension of 556N with tension variation of $\pm$500N. Despite this, the algorithm trued the wheel to its target mean tension within 9N and the improved resulting non-uniformity for all parameters by nearly 500% in a single iteration. Fig. 3.11 shows the wheel state before and after the truing operation and Table 3.2 summarizes the measurements. The maximum variations are 0.17 mm above the mean (lateral), 0.07 mm above the mean (radial), and 104 N below the mean (tension).

Finally, we iterated the truing algorithm to see whether the wheel truing performance improved. The results are summarized in Table 3.3. The non-uniformity improved modestly for every parameter and the mean tension was still within measurement error of the targeted value.

Table 3.2: Truing algorithm results

Parameter	Inital ($\mu \pm \sigma$)	Final ($\mu \pm \sigma$)
Lateral [mm]	0.160 ± 0.736	-0.037 ± 0.107
Radial [mm]	0.050 ± 0.158	-0.046 ± 0.047
Tension [N]	556 ± 211	1009 ± 45

Table 3.3: Second iteration of truing

Parameter	Inital ($\mu \pm \sigma$)	Final ($\mu \pm \sigma$)
Lateral [mm]	-0.037 ± 0.107	0.028 ± 0.073
Radial [mm]	-0.046 ± 0.047	-0.031 ± 0.034
Tension [N]	1009 ± 45	989 ± 39

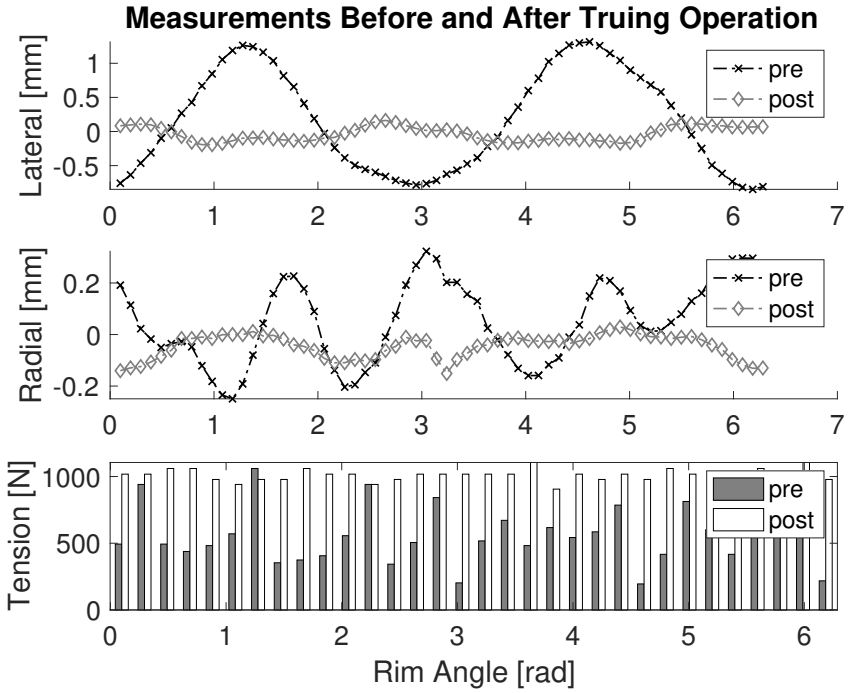

Figure 3.11: The state of the wheel is shown before and after the truing operation. The results are summarized in Table 3.2.

Chapter 4

Conclusion

In this work we demonstrated a method for developing a linear wheel model used for truing and tensioning a bicycle wheel with no *a-priori* knowledge of the mechanical properties of the components. This method can be easily incorporated into existing wheel manufacturing machines provided they have measurement ability for lateral and radial rim displacements, spoke tension measurement capability, and modest computational power. Weighting factors are used to calculate the optimum truing solution and can be adjusted to account for the specification tolerance in the three parameters. Once a characteristic wheel has been modeled this model can be used to efficiently tension and true subsequent wheels of the same design.

Additionally we developed a truing algorithm that minimizes adjustment errors using a prediction of intermediate wheel states after adjustment of each spoke and lateral measurement feedback. This algorithm trues a wheel in a single iteration to any desired tension (within the specification of the wheel components). An important consequence of this approach is that the characterization of the influence functions doesn't rely on an absolute perturbation of the

wheel state because the feedback compensates for this effect during truing and because the model is linear. In practice, therefore, a wheel can be taken from any state, as long as it is partially tensioned, and trued to any tension with only a single adjustment of each spoke (i.e., one complete iteration of the truing algorithm). The time necessary true a wheel is therefore entirely determined by the truing machine and not the initial wheel state. To our knowledge, this is the first publication of such an algorithm along with experimental validation.

The main limitation to the model is the inaccuracy and, perhaps more importantly, the coarse discretization of the tension measurements. As a consequence, the tension parameter is weighted relatively less than the radial and lateral parameters in this work. The resulting wheel state after a truing operation reflects this weighting and therefore the tension errors approach 10%. The main limitation to the truing algorithm is the precision of the spoke tension adjustment but even with the equipment employed here, lateral adjustments were controlled to better than 0.1mm.

Future developments of this work should primarily deal with improving the tension influence functions. The most direct approach is to model the spoke tension influence functions using lateral and radial displacements, the geometry of the wheel, and the measured or calculated spoke stiffness. We did perform an initial evaluation of this approach which showed promise and will be developed in the future. Alternatives are to use different methods to measure spoke tension that have higher resolution and accuracy. One approach that has been suggested ([12]) is to estimate the frequency of the first vibrational mode of the spoke acoustically. Additionally, extending the methods presented here to the case of non-symmetric wheels is a necessary and straightforward exercise for general application to any spoked wheel.

Bibliography

[1] Richard Petrus BegheynEef and Peter Frans Vermeulen. Method and apparatus for aligning a wheel., March 2002.

[2] Jobst Brandt. *The Bicycle Wheel*. Avocet, 1993.

[3] Burgoyne C. J. and Dilmaghanian R. Bicycle Wheel as Prestressed Structure. *Journal of Engineering Mechanics*, 119(3):439–455, March 1993. Publisher: American Society of Civil Engineers.

[4] Mathew Ford. `https://github.com/dashdotrobot/bike-wheel-calc`. [Online; accessed 2-Feb-2019].

[5] Mathew Ford. *Reinventing the Wheel: Stress Analysis, Stability, and Optimization of the Bicycle Wheel*. PhD thesis, Northwestern University, 2018.

[6] Matthew Ford, Patrick Peng, and Oluwaseyi Balogun. Acoustic Modal Testing of Bicycle Rims. *Journal of Nondestructive Evaluation*, 37(1), March 2018.

[7] Henri P. Gavin. Bicycle-Wheel Spoke Patterns and Spoke Fatigue. *Journal of Engineering Mechanics*, 122(8):736–742, August 1996.

[8] Aaron Hunter. Bicycle wheel system identification and optimal truing control for mechatronic systems. In *2020 IEEE/ASME International Conference on Advanced Intelligent Mechatronics (AIM)*, pages 1242–1248, 2020.

[9] Erik Jámbor and Dániel Burmeister. FINITE ELEMENT MODELLING OF THE SPOKE WHEEL TRUING. *ACTA TECHNICA CORVINIENSIS – Bulletin of Engineering*, 9(2):6, apr 2016.

[10] Karel J Keesman. *System identification: an introduction*. Springer Science & Business Media, 2011.

[11] J M Minguez and J Vogwell. An analytical model to study the radial stiffness and spoke load distribution in a modern racing bicycle wheel. *Proceedings of the Institution of Mechanical Engineers, Part C: Journal of Mechanical Engineering Science*, 222(4):563–576, April 2008.

[12] Jeremy J. M. Papadopoulos. Method for trueing spoked wheels, April 1992.

[13] A.J. Sutton Pippard and W.E. Francis. XX. *On a theoretical and experimental investigation of the stresses in a radially spoked wire wheel under loads applied to the rim. The London, Edinburgh, and Dublin Philosophical Magazine and Journal of Science*, 11(69):233–285, February 1931.

[14] N. J. Salamon and R. A. Oldham. Analysis for design of spoked bicycle wheels. *Finite Elements in Analysis and Design*, 10(4):319–333, February 1992.